Multiple time step nonequilibrium molecular dynamics simulation of the rheological properties of liquid *n*-decane

Cite as: J. Chem. Phys. **104**, 255 (1996); https://doi.org/10.1063/1.470896
Submitted: 14 June 1995 • Accepted: 25 September 1995 • Published Online: 31 August 1998

S. T. Cui, P. T. Cummings and H. D. Cochran

Multiple time step nonequilibrium molecular dynamics simulation of the rheological properties of liquid *n*-decane

S. T. Cui, P. T. Cummings,[a] and H. D. Cochran
Department of Chemical Engineering, University of Tennessee, Knoxville, Tennessee 37996-2200 and Chemical Technology Division, Oak Ridge National Laboratory, Oak Ridge, Tennessee 37831-6268

(Received 14 June 1995; accepted 25 September 1995)

Nonequilibrium and equilibrium molecular dynamics simulations are reported for a united-atom model of *n*-decane at a state point in the liquid phase. The viscosity calculated by our nonequilibrium molecular dynamics simulations is in good agreement with that obtained from our equilibrium molecular dynamics simulations via the Green–Kubo relation and with that obtained by Mundy *et al.* [J. Chem. Phys. **102**, 3776 (1995)] using the same potential model at the same state conditions. Additionally, the viscosity calculated by nonequilibrium molecular dynamics is in very good agreement with experimental results for *n*-decane. The algorithm used for the equilibrium molecular dynamics simulations is an application to alkanes of the multitime step Nosé dynamics algorithm developed by Tuckerman and Berne. For the nonequilibrium molecular dynamics simulations, an extension of the multitime step method is derived for the nonequilibrium equations of motion describing planar Couette flow with Nosé thermostat. The contributions of the intramolecular interactions to the stress tensor and its relaxation have been analyzed; the bond stretching motions play a dominant role in the short-time behavior of the atomic stress–stress correlation. © *1996 American Institute of Physics.* [S0021-9606(96)50301-3]

I. INTRODUCTION

The rheological properties of hydrocarbon chain molecules have many important applications in the petrochemical industry. For example, the design of high performance lubricants often requires a good understanding of the detailed molecular level mechanism responsible for the viscous behavior. In this respect, molecular simulation provides a uniquely useful tool for studying these systems. In recent years, a number of molecular simulation studies have been performed on alkanes to study the rheological properties of hydrocarbon chains.[1–8] In these systems, several modes of motion exist corresponding to different time scales spanning over at least an order of magnitude. To achieve efficiency, many of these simulations were carried out by freezing out the fast mode of motion, i.e., fixing the bond distance between the neighboring atoms. This corresponds to a mean fieldlike approach to the effect of the bond stretching on system properties. Although this approach has been generally considered as acceptable, its effect has not been studied in detail, especially on the transient behavior of the stress–stress autocorrelation. In addition, it is desirable to have a method which can incorporate the detailed description of the bond stretching and yet remain efficient computationally. The recent development of the reversible reference system propagator algorithm (rRESPA) by Tuckerman *et al.*[9] has stimulated renewed interest in simulating systems with multiple time scales of motion. Watanabe and Karplus[10] applied the method to alkanes of up to five sites and pentanol in water. Mundy *et al.*[11] used the method to calculate the Newtonian viscosity of liquid *n*-decane using equilibrium molecular dynamics. Xu *et al.*[12] applied the method to a system of bead–spring chains under a shear field.

Two molecular simulation techniques have been commonly used in the calculation of viscosity or transport properties in general; the nonequilibrium molecular dynamics (NEMD) simulation method,[13] which calculates the strain-rate dependent viscosity from which the equilibrium shear viscosity of the system can be obtained by extrapolation to zero shear rate, and the equilibrium molecular dynamics (EMD) simulation based on Green–Kubo theory. The use of NEMD, and to a lesser extent EMD, was recently reviewed by Cummings and Evans.[14] In this paper, we apply the reversible multiple time step method to a system of *n*-decane molecules with interactions modeled by a recently-developed united atom potential (see Sec. II below for details). Both NEMD and EMD simulations are presented. The strain-rate dependent viscosity from NEMD is extrapolated to zero strain rate and is found to be consistent with the viscosity determined from the Green–Kubo relation in the EMD simulation and to agree well with experimental value and with the result of Mundy *et al.*[11] In addition, we analyze the contribution of the intramolecular interaction to the stress tensor and its relaxation. It is found that the bond stretching motions play a dominant role in the short time behavior of the atomic stress–stress autocorrelation.

II. MOLECULAR MODEL AND SIMULATION TECHNIQUES

For a system subject to planar Couette shear flow, the motion of the particles can be described by the SLLOD algorithm which, provided it is appropriately thermostatted, is known to be valid in both the linear and nonlinear response

[a]Author to whom correspondence should be addressed.

regimes.[13] We have developed a multiple time step method based on a phase variable Liouvillean derived from the atomic SLLOD equations of motion.[13] Since the evolution of a system is uniquely determined by its Liouvillean, the method does not depend on the existence of a Hamiltonian. The details of derivation of the method are given in the Appendix. The thermostat employed is an atomic thermostat [see Eq. (A1) of the Appendix]. Recently, Travis *et al.*[15] published a study of the effects of atomic and molecular thermostats on the nonlinear properties of a rigid molecular system (homonuclear diatomics) described by SLLOD dynamics. They showed that at high strain rate (reduced strain rates $\geqslant 2$) differences in the strain-rate dependent shear viscosities are evident. The simulations reported in this paper are all at reduced strain rates of unity or less, where atomic and molecular thermostatting mechanisms produce essentially the same results. Additionally, we note that the Newtonian viscosity is, in principle, independent of the thermostatting mechanism used. The relative merits of atomic and molecular thermostats on nonrigid chain molecules will be discussed at greater length in a subsequent publication.

The model we used for *n*-decane is the model used previously by Mundy *et al.*[11] and also by Siepmann *et al.*[16,17] in their successful prediction of phase equilibria in the normal alkanes using the Gibbs ensemble Monte Carlo method. It is a united atom model (i.e., methyl and methylene groups treated as spherical interaction sites) with the interaction centers located at the center of the carbon atoms. The model has been described in detail in the published literature.[16,17] Here, we briefly describe the salient features of the model. The interaction between atoms on different molecules and atoms separated by more than three bonds in the same molecule is described by a Lennard-Jones potential,

$$u_{ij}(r)=4\epsilon_{ij}\left[\left(\frac{\sigma_{ij}}{r}\right)^{12}-\left(\frac{\sigma_{ij}}{r}\right)^{6}\right],$$

where ϵ_{ij} is the well depth and σ_{ij} the zero point of the potential between a site of type i and a site of type j. All the atoms in a chain have the same Lennard-Jones size parameter $\sigma_i \equiv \sigma_{ii}=3.93$ Å the well depth parameters are $\epsilon_i/k_B \equiv \epsilon_{ii}/k_B=114$ K for interactions between end atoms and $\epsilon_i/k_B=47$ K for interactions between internal atoms. Boltzmann's constant is here denoted k_B. The Lorentz–Berthelot combining rules [$\epsilon_{ij}=(\epsilon_i\epsilon_j)^{1/2}$, $\sigma_{ij}=(\sigma_i+\sigma_j)/2$] are used for interactions between an end atom and an internal atom. The bond bending interaction is described by a harmonic potential with an equilibrium angle of $\theta=114°$ and a force constant of $A/k_B=62\,500$ K/rad^2. The torsional interaction is described by the potential developed by Jorgensen *et al.*[18] The bond stretching is also described by a harmonic potential,[11] with the equilibrium bond distance $d=1.54$ Å, and a force constant of $B/k_B=452\,900$ K/Å^2. A cutoff distance of 2.5σ is used for all the Lennard-Jones interactions.

We carried out the simulations at absolute temperature $T=480$ K and density of 0.6136 g/cm^3, the same state point as in the work of Mundy *et al.*[11] For the EMD simulations, the multiple time step method developed by Tuckerman *et al.*[9] is used with a simple Nosé thermostat on the atomic degrees of freedom. Other more sophisticated thermostats have been developed to address nonergodicity problems for systems which are very rigid (such as proteins) or which have few degrees of freedom.[11,19] For the liquid normal decane studied here, these problems are not encountered so that the use of the simpler Nosé thermostat is well-justified. For the calculation of the strain-rate dependent viscosity, a multiple time step NEMD method is used which is described in detail in the Appendix. A time step of 2.35 fs is used for the slow mode motion and a time step of 0.235 fs is used for the fast motion. The system consists of 100 *n*-decane molecules. The simulation is started by putting the centers of mass of the decane molecules on the lattice points, and all molecules in the trans conformation. Each atom is given a very small initial Lennard-Jones diameter of 0.05σ and the atom is grown to its full size during an EMD simulation of 44.7 ps in length. During the particle growth process, the bond stretching, bond bending, and torsional potentials are active so the equilibrium intramolecular structure is not affected. A similar procedure was used to create the initial configuration in the molecular simulation of liquid *n*-butane.[20] To efficiently remove the heat produced during the particle growth process, the velocity of the particles is rescaled to the prescribed temperature every 10 large time steps. After the particles grow to their full size, an additional 250 ps of equilibration is performed using EMD with the velocity rescaling scheme. The configuration produced from the equilibration run is used as the starting configuration for an additional 988 ps equilibration run using the multiple time step with the Nosé thermostat. In all simulations reported in this paper, a Nosé thermostat time constant $\tau=0.3$ ps is used. The production runs of EMD and NEMD simulation start from the configuration produced by this process.

III. THEORY

In a NEMD calculation, the strain-rate dependent viscosity η is determined from the constitutive relation

$$\eta=-\frac{\langle P_{xy}\rangle}{\gamma}, \tag{1}$$

where $\langle P_{xy}\rangle$ is the average of the xy component of the pressure tensor $\mathbf{P}$ and γ is the strain rate characterizing the shear field. We have chosen the x direction to be the flow direction and y direction to be the flow gradient direction, so that $\gamma=\partial u_x/\partial y$, where u_x is the streaming velocity in the x direction. The pressure tensor $\mathbf{P}$ can be calculated using either the atomic, $\mathbf{P}^{(a)}$, or the molecular, $\mathbf{P}^{(m)}$, formalisms, which are given by

$$\mathbf{P}^{(a)}V=\sum_{i,a} m_{ia}\mathbf{v}_{ia}\mathbf{v}_{ia}+\frac{1}{2}\underbrace{\sum_{i,a}\sum_{j,b}}_{i\neq j}(\mathbf{r}_{ia}-\mathbf{r}_{jb})\mathbf{f}_{ia,jb}$$

$$+\sum_{i,a}\delta\mathbf{r}_{ia}\mathbf{f}_{ia}^{(\mathrm{intra})}, \tag{2a}$$

$$\mathbf{P}^{(m)}V=\sum_i m_i\mathbf{v}_i\mathbf{v}_i+\frac{1}{2}\underbrace{\sum\sum}_{i\neq j}(\mathbf{r}_i-\mathbf{r}_j)\mathbf{F}_{ij}, \tag{2b}$$

where the indices i and j refers to molecules i and j, indices a and b refer to interactions sites a and b in molecules i and j, respectively, $\mathbf{f}_{ia,jb}$ is the interaction force between site a in molecule i and site b in molecule j, $\delta\mathbf{r}_{ia}$ is the position vector of site a in molecule i relative to the center of mass of molecule i, $\mathbf{f}_{ia}^{(\mathrm{intra})}$ is the total intramolecular force on site a in molecule i, m_{ia}, $\mathbf{r}_{ia}$, and $\mathbf{v}_{ia}$ are the mass, position, and velocity, respectively, of site a in molecule i, $\mathbf{F}_{ij}$ is the total force on molecule i and due to molecule j, and m_i, $\mathbf{r}_i$, and $\mathbf{v}_i$ are the mass, position, and velocity, respectively, of molecule i. Note that since the total intramolecular force sums to zero for a given molecule, the last term in Eq. 2(a) does not depend on the choice of origin in the determination of $\delta\mathbf{r}_{ia}$, so this can be conveniently chosen to be the center of mass of the molecule. When the molecular pressure tensor formalism is used in a simulation, the symmetric part of the $P_{xy}^{(m)}$ is used in Eq. (1) to calculate the viscosity.[21,22]

In an EMD simulation, the viscosity is calculated according to the Green–Kubo theory,

$$\eta=\frac{V}{k_BT}\int_0^\infty dt\langle P_{xy}(t)P_{xy}(0)\rangle. \tag{3}$$

In this equation, $\langle P_{xy}(t)P_{xy}(0)\rangle$ is the correlation function of the xy component of the pressure tensor. As in Eq. (1), the symmetric part of the pressure tensor is implied when the molecular form of the pressure tensor is used in Eq. (3).

In the absence of an external field, the system is isotropic so that the xy, yz, and xz components are equivalent and use of all the three off-diagonal elements improves the statistics. In a recent publication, Daivis and Evans[8] showed that the tensorial property of the viscosity coefficient allows the use of all elements of the pressure tensor in the calculation of the viscosity, so that

$$\eta=\frac{V}{10k_BT}\int_0^\infty dt\langle\mathbf{P}^{0s}(t)\cdot\mathbf{P}^{0s}(0)\rangle, \tag{4}$$

where $\mathbf{P}^{0s}(t)$ denotes the symmetric traceless part of the pressure tensor and the operator $\cdot$ implies the double contraction of two second rank tensors.

IV. RESULTS

In Fig. 1(a), we have plotted the strain-rate dependent viscosity of *n*-decane at $T=480$ K and density of 0.6136 g/cm^3, the same state point studied by Mundy *et al.*[11] The shear rate γ is shown in reduced units $\gamma(m\sigma^2/\epsilon)^{1/2}$. Detailed numerical data and production run lengths are tabulated in Table I. The results are obtained by block averaging with each block consisting of 47 ps simulation segment. The collection of simulation results for block averaging does not begin until the system has reached steady state. The time to reach steady state is estimated as the greater of two times: the longest relaxation time [the rotational relaxation time which is about 10 ps (Ref. 23)] and the time taken for the a molecule at the top of the simulation cell to have traversed the simulation cell twice. For shear rates $\gamma\geqslant 0.09$, the latter times turns out to be equal or less than 40 ps, so the data collection is started 47 ps after shearing. For $\gamma=0.04$, the data collections begins 117.5 ps after shearing. Since our runs are relatively long, the average is not affected much by a small change in the exact time where the data collection starts. The figure shows viscosity plotted as a function of the 1/2 power of strain rate since from kinetic and mode coupling theories[24–26] it is known that the strain rate dependence of the shear viscosity is linear in $\gamma^{1/2}$. As shown in the figure, the shear viscosity varies essentially linearly as the square root of the shear rate. The extrapolation to the zero shear rate gives a zero strain rate (i.e., Newtonian) viscosity of $\eta_0=(197\pm3)\times10^{-6}$ Pa s. The error is estimated by assuming the strain rate dependent viscosities can be regarded as exact and performing linear regression on the data and estimating the error in the intercept using standard regression techniques.[27] This leads to an underestimate of the error in the NEMD simulation. On the other hand, the smallness of the estimated error is an indication of the high degree to

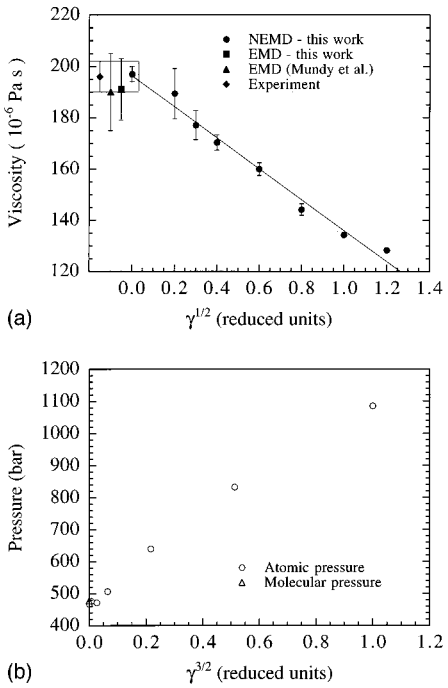

FIG. 1. (a) The strain rate dependent shear viscosity for liquid *n*-decane at temperature $T=480$ K and density of $\rho=0.6136$ g/cm^3 as a function of $\gamma^{1/2}$. The line is a least-squares linear fit to the NEMD simulation results. The error bars for the two largest strain rate data points are smaller than the symbol. At the left-hand side of the graph, the three simulation results [extrapolated NEMD, EMD from this work and EMD from Mundy *et al.* (Ref. 11)] are shown along with the experimental result. For clarity, the simulation results and experiment are separated from one another whereas in fact all should be plotted at $\gamma^{1/2}=0$. The shaded region shows the range of viscosity within the estimated error of the experimental result. (b) The shear dilatancy of the normal decane from the same simulation as in (a). The nonzero strain rate points are calculated using the atomic stress tensor. The statistical uncertainties for all the points in the figure are smaller than the symbols. At zero strain rate, the values for the pressure from the atomic and molecular tensor formalism are essentially indistinguishable.

TABLE I. The viscosity and pressure at various strain rates obtained from the NEMD and EMD simulations. The pressure values shown in the table do not include the long range correction. The numbers in the parentheses represent the estimated statistical uncertainty based on block averages. The run length in the last column is the production run length during which data collection is performed. For NEMD, this does not include time for the system to reach the steady state. See text for details.

γ	η (10^{-6} Pa s)	P (bar)	Run length (ps)
	197(3)[a]	468(6)[d]	
0 (EMD)	191(12)[b]	478(6)[e]	2326
	196(5)[c]		
0.04	189.4(9.9)	477(4)	2233
0.09	177.2(5.7)	473(6)	1128
0.16	170.4(3.0)	507(6)	1105
0.36	160.0(2.5)	640(5)	423
0.64	144.2(2.3)	833(10)	317
1.00	134.3(0.9)	1086(10)	293
1.44	128.3(0.7)	1315(20)	188

[a]The viscosity based on the linear extrapolation of the NEMD calculation of the strain rate dependent viscosity, assuming the shear viscosity is linear in $\gamma^{1/2}$. The uncertainty indicated in the parentheses includes only the statistical uncertainty resulting from the linear regression and does not take into account the statistical uncertainty in the data. See text for details.
[b]The viscosity obtained from integrating the stress–stress autocorrelation function in the EMD simulation.
[c]The experimental viscosity for *n*-decane at $T=480$ K and pressure of 120 bar. The error estimates are based on the viscosity at $T=480$ K and pressures of 100 and 140 bar.
[d]The pressure obtained in EMD using the atomic pressure tensor formalism.
[e]The pressure obtained in EMD using the molecular pressure formalism.

which the strain rate dependent viscosities fit the linear function of $\gamma^{1/2}$ as shown in Fig. 1(a). Although there is some disagreement about whether this simple extrapolation procedure is valid in all cases, alternative extrapolations (e.g., Cummings and Morriss[28] and Chynoweth *et al.*,[5] and Berker *et al.*[7] investigated alternative extrapolations) suggest that the result obtained by linear extrapolation is quite consistent with other extrapolation routes. In any event, given the relatively weak dependence of the simulation results on strain rate, we expect the error resulting from the choice of the extrapolation procedure itself to be small. This is also supported by our calculation of the Newtonian viscosity from the integration of the molecular stress–stress autocorrelation function, which gives a value of $\eta_0=(191\pm12)\times10^{-6}$ Pa s. This compares very well with the work of Mundy *et al.*[11] who reported a value of $\eta_0=(190\pm15)\times10^{-6}$ Pa s obtained by EMD for the same state point. The experimental values of the viscosity are obtained under the constant pressure condition. For pressures in the range 100–140 bar, the experimental viscosity is in the range[29] $\eta_0=(196\pm6)\times10^{-6}$. It appears that our NEMD result is in excellent agreement with the experimental data. The equilibrium viscosity calculated from the Green–Kubo formula is slightly smaller than the linear extrapolation of the NEMD result, but still in excellent agreement with NEMD result within the statistical uncertainty.

We show in Fig. 1(b) the dependence of pressure on shear rate. The numerical values are tabulated in Table I. At high strain rate, the error bars are smaller than the symbols in the figure. For the NVT simulations it is known that the hydrostatic pressure, $p=(1/3)\mathrm{Tr}(\mathbf{P})$, where Tr denotes trace, satisfies the asymptotic relation.[24–26,30–33]

$$p=p_0+p_1\gamma^{3/2}. \tag{5}$$

Consequently, the pressure in Fig. 1(b) is plotted as a function of $\gamma^{3/2}$. Figure 1(b) shows that for the range of shear rate studied in this work, the $\gamma^{3/2}$ power law describes the results very well for the shear rate between 0 and 1. Also included in the figure are the pressure data from the equilibrium simulation obtained from runs of 2326 ps. Both atomic and molecular expressions have been used in the calculation of the equilibrium pressure. The calculated pressure values from the molecular formalism and the atomic formalism give values which are in excellent agreement with each other and with the extrapolation of the NEMD calculation to zero shear rate. None of the points shown in Fig. 1(b) includes the long range correction which is -352 bar for the cutoff distance 2.5σ for the equilibrium system at the state point studied in this work. When the long range corrections are included, the calculated equilibrium pressure for *n*-decane at the state point studied in this work are $p^{(a)}=116\pm6$ bar and $p^{(m)}=126\pm6$ bar. These values appear to be slightly lower than the pressure value of 168 ± 10 bar obtained by averaging three different runs in the work of Mundy *et al.*[11] However, these authors used a larger cutoff distance, 3.5σ. In their paper, they reported a long range correction to their pressure of -63 atm. We have been unable to confirm this value and by our calculation the correction should be -128 bar for a cutoff distance of 3.5σ. Using this value for the long range correction, we find that Mundy *et al.*'s pressure should be 103 ± 10 bar in good agreement with our results.

Figures 2(a) and 2(b) show the Newtonian viscosity calculated from the Green–Kubo theory using the molecular tensor formalism. Figure 2(a) shows the integrals obtained using Eqs. (3) and (4) while Fig. 2(b) shows the stress–stress autocorrelation functions themselves. The results are obtained from a long simulation run of 2326 ps. In the calculation of the correlation functions, we sampled the data every 10 large time steps, so that the stress–stress autocorrelation function in a single run was calculated using 97 000 time origins. It can be seen from Fig. 2(a) that after reaching a plateau value in about 10 ps (which coincides with the rotational relaxation time of approximately 10 ps), the integral is essentially flat with some statistical fluctuation. The viscosity value from Fig. 2(a) varies in between 179×10^{-6} Pa s and 203×10^{-6} Pa s. The midpoint corresponds to a viscosity value of 191×10^{-6} Pa s. This is the basis for our estimate, reported above, that the Green–Kubo calculation gives a viscosity value of $(191\pm12)\times10^{-6}$ Pa s in very good agreement with the NEMD simulation and the calculation of Mundy *et al.*[11] who report a value of $(190\pm15)\times10^{-6}$ Pa s. Their result is obtained from averaging three independent runs of each 900 ps, so that the total run length is comparable to ours.

In principle, the Newtonian viscosity could also be calculated in an EMD simulation using the atomic pressure tensor, Eq. (2a), of the Green–Kubo relations. We have shown

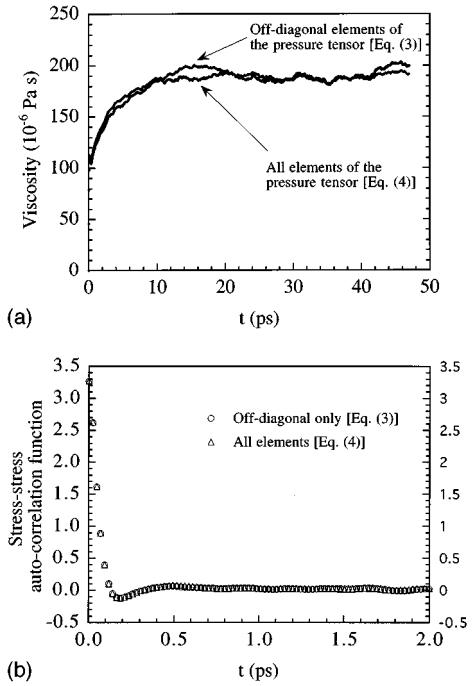

FIG. 2. (a) The shear viscosity calculated from integrating the molecular stress–stress autocorrelation functions using Eqs. (3) and (4) as a function of the upper integral time limit t. The arrows indicate the curve obtained using the three independent off diagonal elements of the symmetric molecular stress tensor [Eq. (3)] and the curve obtained using all the elements of the symmetric traceless molecular tensor [Eq. (4)]. See text for details. (b) The short time behavior of the molecular stress–stress autocorrelation functions which are the integrands of the integrals shown in (a). The circles are the result of averaging the stress–stress autocorrelation functions of the three independent off diagonal elements of the symmetric molecular stress tensor [Eq. (3)]. The triangles are the result of using all the elements of the symmetric traceless molecular stress tensor [Eq. (4)]. The correlation functions are in reduced units.

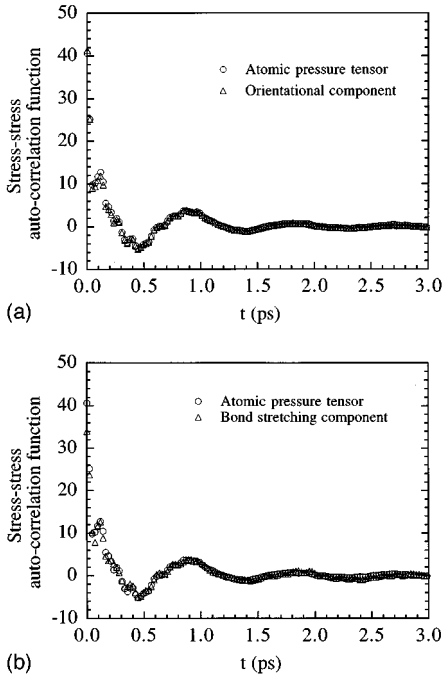

FIG. 3. (a) The short time behavior of the atomic stress–stress autocorrelation function compared to the orientational component. The figure is drawn in reduced units. Note the magnitude difference at time zero in comparison to the molecular stress–stress autocorrelation functions shown in Fig. 2(b), and also the oscillatory behavior of the correlation function. (b) Comparison of the atomic stress–stress autocorrelation function with its bond stretching component. The same atomic stress–stress autocorrelation function in (a) is redrawn here. The figure shows that both the large magnitude of the atomic stress–stress autocorrelation function and its oscillatory behavior are essentially due to the bond stretching component of the atomic forces.

in Fig. 1(b) that the pressures resulting from the atomic and molecular expressions for the pressure tensor are the same in accordance with theory.[34] Unlike the calculation of the pressure in EMD or NEMD, or the NEMD expression of the viscosity, which are both linear in the pressure tensor, the Green–Kubo relations are quadratic in the pressure tensor elements and this product may contain slowly decaying components. The equivalence between the atomic pressure tensor and molecular pressure tensor formalism in calculating the transport coefficient has been studied by a number of authors. Maréchal and Ryckaert[35] showed that the transport coefficients obtained from the two formalisms are the same in the long time limit. The difference between partial integrals of the atomic and molecular stress–stress autocorrelation functions involves a slow decaying component which is proportional to $t^{-1/2}$. Allen[36] showed explicitly that the atomic stress tensor and the molecular stress tensor differ by a component which is the second derivative of a tensor θ called by him the orientational tensor, i.e.,

$$\mathbf{P}^{(a)}=\mathbf{P}^{(m)}+\tfrac{1}{2}\ddot{\theta}, \tag{6}$$

where $\mathbf{P}^{(m)}$ is the symmetric part of the molecular tensor,

$$\ddot{\theta}=\sum_{i,a}\ \delta\mathbf{r}_{ia}\mathbf{f}_{ia}^{(\mathrm{total})}+\sum_{i,a}\ \mathbf{f}_{ia}^{(\mathrm{total})}\delta\mathbf{r}_{ia}+2\sum_{i,a}\ \delta\mathbf{r}_{ia}\delta\mathbf{r}_{ia} \tag{7}$$

is the second derivative of the orientational tensor defined as

$$\theta=\sum_{i,a}\ m_{ia}\delta\mathbf{r}_{ia}\delta\mathbf{r}_{ia}\,. \tag{8}$$

$\mathbf{f}_{ia}^{(\mathrm{total})}$ is the total force acting on atom a in molecule i. The atomic and molecular tensor autocorrelation functions are then related by

$$\langle p_{\alpha\beta}^{(a)}(t)p_{\alpha\beta}^{(a)}(0)\rangle=\langle p_{\alpha\beta}^{(m)}(t)p_{\alpha\beta}^{(m)}(0)\rangle+\langle\ddot{\theta}_{\alpha\beta}(t)p_{\alpha\beta}^{(m)}(0)\rangle+\tfrac{1}{4}\langle\ddot{\theta}_{\alpha\beta}(t)\ddot{\theta}_{\alpha\beta}(0)\rangle. \tag{9}$$

Allen[36] also suggested that the last term in Eq. (9) has a long time algebraic decaying component. For the *n*-decane system studied here, we find that both the molecular stress–stress autocorrelation function and the cross-correlation functions are small in comparison to the atomic stress–stress autocorrelation function and the reorientational component $\ddot{\theta}$. Figure 3(a) shows this behavior. For clarity, we show only the atomic stress–stress autocorrelation function and the reorien-

tational correlation function. It can be seen that the atomic correlation function is dominated by the contribution from the reorientational component over the time frame shown (3 ps). It should also be noted that the atomic stress–stress autocorrelation function exhibits oscillatory behavior evidently driven by the reorientational component.

To understand this behavior, we studied the contributions to the total atomic stress tensor from the intermolecular, bond stretching, bond-angle bending, and the torsional forces. (By comparison to these four classes of interactions, the intramolecular Lennard-Jones forces make a negligible contribution to the atomic stress tensor.) We expect the cross correlation between motions induced by these forces to be small as they correspond to the motions on different time scales. We find that the bond stretching component of the stress–stress autocorrelation function is by far the largest component. At time $t=0$, it is about an order of magnitude larger than bond-angle bending contribution. The torsional contribution is negligibly small by comparison. Figure 3(b) shows the total atomic stress–stress autocorrelation function and the bond stretching component. It is clear that these two quantities are nearly the same in magnitude and that the oscillatory behavior in both coincide. This suggests that the atomic stress–stress autocorrelation function is dominated by its bond stretching component and the rate at which this component decays determines the accuracy of the EMD calculation of the viscosity using the atomic pressure tensor formalism in the Green–Kubo relation.

In their study of *n*-butane, Maréchal *et al.*[1] showed that the viscosity calculated from the atomic and molecular formalisms was the same. The difference between their model and the one studied in this paper is that in our case a bond stretching force is used to impose the bond distance constraints, while in their work the bond distance was rigidly fixed, and as shown in the preceding paragraph, the bond-stretching component of the atomic stress–stress autocorrelation function is the dominant contribution to the difference between the atomic and molecular expressions at short times. The chain length is also a contributing factor, as the elastic stress related to the bond stretching will obviously increase as the chains get longer. Consequently, there is no conflict between the current findings and those of Maréchal *et al.*

V. CONCLUSIONS

In summary, we have applied a reversible multiple time step method to an united atom model of liquid *n*-decane. The model includes bond stretching, bond-angle bending, and torsional potentials. We studied the rheological property of the *n*-decane liquid by both NEMD simulation and EMD simulation. The zero shear rate extrapolation of the shear rate dependent viscosity of the *n*-decane agree well with our calculation from the EMD simulation using the Green–Kubo formalism. Our calculation predicts an equilibrium viscosity which is in close agreement with experimental data for the potential model used for liquid normal decane in this study. The short time atomic stress–stress autocorrelation function is found to be very different from the molecular stress–stress autocorrelation function. This difference comes predominantly from the bond stretching component of the stress–stress autocorrelation function.

ACKNOWLEDGMENTS

The work of H.D.C. has been supported by the Division of Chemical Sciences of the U.S. Department of Energy under Contract No. DE-AC-840R21400 with Lockheed Martin Energy Systems, Inc. The authors gratefully acknowledge support of this research at Oak Ridge National Laboratory by a Laboratory Director's Research and Development grant entitled ''Molecular-Based Study of Fluids and Amorphous Materials Using Parallel Supercomputers.'' A description of this project is available on the World Wide Web at the location http://flory.engr.utk.edu/ldrd/w.html. Computational facilities have been provided by the Center for Computational Sciences at Oak Ridge National Laboratory. Helpful discussions with Dr. Peter Daivis of the Australian National University and Mr. Ravi Bhupathiraju of the University of Tennessee are gratefully acknowledged. We thank Dr. Mundy, Dr. Klein, and Dr. Siepmann for providing us with a preprint of their ongoing work on *n*-decane prior to publication.

APPENDIX

The SLLOD equations of motion for a system under planar Couette flow is given by

$$\begin{aligned}
\dot{\mathbf{r}}_{ia} &= \frac{\mathbf{p}_{ia}}{m_{ia}} + \gamma y_{ia}\hat{x}, \\
\dot{\mathbf{p}}_{ia} &= \mathbf{F}_{ia} - \gamma p_{y,ia}\hat{x} - \dot{\zeta}\mathbf{p}_{ia}, \\
\dot{\zeta} &= \frac{p_\zeta}{Q}, \\
\dot{p}_\zeta &= F_\zeta,
\end{aligned} \tag{A1}$$

where $\mathbf{r}_{ia}$ and $\mathbf{p}_{ia}$ are the vector coordinates and peculiar momentum of atom a in molecule i, y_{ia} and $p_{y,ia}$ are its y components, m_{ia} the mass, $\hat{x}$ is a unit vector in x direction, ζ, p_ζ, and Q are the variables related to the Nosé thermostat,

$$F_\zeta = \sum_{i,a} \frac{p_{ia}^2}{m_{ia}} - 3Nk_BT, \quad Q = 3Nk_BT\tau^2,$$

τ is the Nosé thermostat time constant, and N is the total number of atoms in the system.

From the SLLOD equation of motion, we can form the Liouvillean of the system which govern its evolution in time. Since we are interested in the evolution of the phase variable, we obtain the phase variable Liouvillean

$$iL=\sum_i \dot{\mathbf{r}}_i\cdot\frac{\partial}{\partial\mathbf{r}_i}+\sum_i \dot{\mathbf{p}}_i\cdot\frac{\partial}{\partial\mathbf{p}_i}+\dot{\zeta}\frac{\partial}{\partial\zeta}+\dot{p}_\zeta\frac{\partial}{\partial p_\zeta}$$
$$=\sum_i \frac{\mathbf{p}_i}{m_i}\cdot\frac{\partial}{\partial\mathbf{r}_i}+\gamma\sum_i y_i\cdot\frac{\partial}{\partial x_i}+\sum_i \mathbf{F}_i\cdot\frac{\partial}{\partial\mathbf{p}_i}$$
$$-\gamma\sum_i p_{yi}\cdot\frac{\partial}{\partial p_{xi}}-\dot{\zeta}\sum_i \dot{\mathbf{p}}_i\cdot\frac{\partial}{\partial\mathbf{p}_i}+\dot{\zeta}\frac{\partial}{\partial\zeta}+\dot{p}_\zeta\frac{\partial}{\partial p_\zeta}, \quad \text{(A2)}$$

where for simplicity of notation we use i to refer to the ith atom in the system. Our decomposition of the Liouvillean is based on the realization that the time scale of the shearing motion encountered in a simulation is usually comparable to the translational motion of the particles in the system, while the intramolecular motion is much faster. The fastest intramolecular motion, the bond stretching, is at least an order of magnitude faster than the translational motion. We thus choose as our reference system Liouvillean

$$iL_r=\sum_i \frac{\mathbf{p}_i}{m_i}\cdot\frac{\partial}{\partial\mathbf{r}_i}+\sum_i \mathbf{F}_{ri}\cdot\frac{\partial}{\partial\mathbf{p}_i}, \quad \text{(A3)}$$

where $\mathbf{F}_{ri}$ includes all the forces on atom i except the intermolecular force. The remaining part of the Liouville operator is given by

$$i\Delta L=iL-iL_r=\gamma\sum_i y_i\cdot\frac{\partial}{\partial x_i}+\sum_i \mathbf{f}_i\cdot\frac{\partial}{\partial\mathbf{p}_i}-\gamma\sum_i p_{yi}\cdot\frac{\partial}{\partial p_{xi}}-\dot{\zeta}\sum_i \dot{\mathbf{p}}_i\cdot\frac{\partial}{\partial\mathbf{p}_i}+\dot{\zeta}\frac{\partial}{\partial\zeta}+\dot{p}_\zeta\frac{\partial}{\partial p_\zeta}, \quad \text{(A4)}$$

where $\mathbf{f}_i=\mathbf{F}_i-\mathbf{F}_{ri}$ includes all the intermolecular forces acting on atom i. More sophisticated decompositions could introduce several time scales corresponding to different kind of intramolecular motions (bond stretching, bond bending, and torsional) and translational motion. The largest time scale is set by the slowest motion, i.e., the translational motion, while the smallest time scale is set by the bond stretching, which is the fastest motion. We choose to use only two time scales for simplicity. Using notation similar to that in Tuckerman *et al.*,[9] the time propagator for our system is

$$G(\Delta t)=\exp\left[\frac{\Delta t}{2}F_\zeta(p_\zeta)\frac{\partial}{\partial p_\zeta}\right]\exp\left[\frac{\Delta t}{4}\mathbf{f}(\mathbf{r})\cdot\frac{\partial}{\partial\mathbf{p}}\right]\exp\left[-\frac{\Delta t}{2}\dot{\zeta}\mathbf{p}\cdot\frac{\partial}{\partial\mathbf{p}}\right]\exp\left[\frac{\Delta t}{4}\mathbf{f}(\mathbf{r})\cdot\frac{\partial}{\partial\mathbf{p}}\right]\exp\left[\frac{\Delta t}{2}\dot{\zeta}\cdot\frac{\partial}{\partial\zeta}\right]$$
$$\times\exp\left[-\frac{\Delta t}{2}\gamma p_y\cdot\frac{\partial}{\partial p_x}\right]\exp\left[\frac{\Delta t}{2}\gamma y\cdot\frac{\partial}{\partial x}\right]\exp(iL_r\Delta t)\exp\left[\frac{\Delta t}{2}\gamma y\cdot\frac{\partial}{\partial x}\right]\exp\left[-\frac{\Delta t}{2}\gamma p_y\cdot\frac{\partial}{\partial p_x}\right]$$
$$\times\exp\left[\frac{\Delta t}{2}\dot{\zeta}\cdot\frac{\partial}{\partial\zeta}\right]\exp\left[\frac{\Delta t}{4}\mathbf{f}(\mathbf{r})\cdot\frac{\partial}{\partial\mathbf{p}}\right]\exp\left[-\frac{\Delta t}{2}\dot{\zeta}\mathbf{p}\cdot\frac{\partial}{\partial\mathbf{p}}\right]\exp\left[\frac{\Delta t}{4}\mathbf{f}(\mathbf{r})\cdot\frac{\partial}{\partial\mathbf{p}}\right]\exp\left[\frac{\Delta t}{2}F_\zeta(p_\zeta)\frac{\partial}{\partial p_\zeta}\right], \quad \text{(A5)}$$

where, for simplicity, we have dropped the atom index i since every atom will have the same propagator, and

$$\exp(iL_r\Delta t)=\left\{\exp\left[\frac{\delta t}{2}\mathbf{F}_r(\mathbf{r})\cdot\frac{\partial}{\partial\mathbf{p}}\right]\exp\left[\delta t\frac{\mathbf{p}}{m}\cdot\frac{\partial}{\partial\mathbf{r}}\right]\times\exp\left[\frac{\delta t}{2}\mathbf{F}_r(\mathbf{r})\cdot\frac{\partial}{\partial\mathbf{p}}\right]\right\}^n. \quad \text{(A6)}$$

is the reference propagator. Here, Δt is the large time step and δt is the small time step which are related by $\Delta t=n\,\delta t$, where n is an integer. It is noted that the propagator within the braces produces the standard velocity Verlet algorithm.

We now apply propagator Eq. (A5) to the set of initial phase variables $[\mathbf{r}(0),\mathbf{p}(0),\zeta(0),p_\zeta(0)]$ using the formulas

$$\exp\left(c\frac{\partial}{\partial q}\right)f(q)=f(q+c) \quad \text{(A7)}$$

and

$$\exp\left(-\frac{\Delta t}{2}\dot{\zeta}p\frac{\partial}{\partial p}\right)\phi(p)=\phi\left[p\exp\left(-\frac{\Delta t}{2}\dot{\zeta}\right)\right]. \quad \text{(A8)}$$

Note that, for planar Couette flow, the x and y components of the peculiar momenta are independent of each other and that Eq. (A7) applies when the operator $\exp[-(\Delta t/2)\gamma p_y\partial/\partial p_x]$ acts on the momentum variable. We then obtain the following formulas for updating the phase variables:

$$\mathbf{r}(\Delta t)=\mathbf{r}_r(\Delta t,\mathbf{r}_0,\mathbf{v}_0)+\frac{\Delta t}{2}\gamma y_r(\Delta t,\mathbf{r}_0,\mathbf{v}_0)\hat{x},$$
$$\mathbf{v}(\Delta t)=\left[\mathbf{v}_r(\Delta t,\mathbf{r}_0,\mathbf{v}_0)+\frac{\Delta t}{4m}\mathbf{f}(\Delta t)\right]\exp\left(-\frac{\Delta t}{2}\dot{\zeta}_0\right)+\frac{\Delta t}{4m}\mathbf{f}(\Delta t)-\frac{\Delta t}{2}\gamma v_{yr}(\Delta t,\mathbf{r}_0,\mathbf{v}_0)\times\exp\left(-\frac{\Delta t}{2}\dot{\zeta}_0\right)\hat{x}, \quad \text{(A9)}$$

where

$$\mathbf{r}_0=\mathbf{r}(0)+\frac{\Delta t}{2}\gamma y(0)\hat{x},$$
$$\mathbf{v}_0=\left[\mathbf{v}(0)+\frac{\Delta t}{4m}\mathbf{f}(0)\right]\exp\left(-\frac{\Delta t}{2}\dot{\zeta}_0\right)+\frac{\Delta t}{4m}\mathbf{f}(0)-\frac{\Delta t}{2}\gamma v_{y0}\hat{x}, \quad \text{(A10)}$$

$$\dot{\zeta}_0 = \dot{\zeta}(0) + \frac{\Delta t}{2Q} F_{\dot{\zeta}}[p(0)],$$

where the subscript r refers to "reference system" and we have replaced momentum $\mathbf{p}$ with $\mathbf{v}$ using the relation $\mathbf{p}=m\mathbf{v}$ and v_{y0} is the y-component of $\mathbf{v}_0$. The variables ζ and $\dot{\zeta}$ are integrated by the usual velocity Verlet algorithm

$$\begin{aligned} \zeta(\Delta t) &= \zeta(0) + \Delta t \dot{\zeta}(0) + \frac{\Delta t^2}{2Q} F_{\dot{\zeta}}[p(0)], \\ \dot{\zeta}(\Delta t) &= \dot{\zeta}(0) + \frac{\Delta t}{2Q} \{F_{\dot{\zeta}}[p(0)] + F_{\dot{\zeta}}[p(\Delta t)]\}. \end{aligned} \tag{A11}$$

We observe that when the shear rate is set to zero, Eqs. (A9) and (A10) reduce to Eqs. (7.9) and (7.10) of Tuckerman *et al.*[9]

We are also developing a version of the multitime step algorithm for a Nosé thermostat applied only to the translational kinetic energy of the center of mass of the molecules which will be evaluated in a future publication. Differences between thermostating the atomic and center of mass translational motion may lead to differences in rheological properties at very high shear rate.[15]

A multitime step algorithm for a bead–spring system NEMD was developed independently by Xu *et al.*[12] The main difference between our approach and theirs is that in our decomposition of the total Liouvillean of the system, the shearing motion has been decomposed into the part involving the weaker intermolecular interaction in both coordinate and velocity equations of motion, in accordance with the general multitime steps approach of decomposing the different modes of motion. In the work of Xu *et al.*, the coordinate part of the shearing motion is decomposed into the intramolecular motion while the momentum part of the shearing motion is decomposed into the intermolecular motion. Another minor difference is that in the work of Xu *et al.*, the strain rate term in their derivation of the multitime algorithm is treated in an approximate manner. This is unnecessary for the particular case of planar Couette flow considered here since the strain rate term involves different components of the momentum, with the consequence that the strain rate term needs not be exponentiated. This would not be the case in other flow geometries such as extensional flow.

[1] G. Maréchal, J.-P. Ryckaert, and A. Bellemans, Mol. Phys. **61**, 33 (1987).
[2] J. H. R. Clarke and D. Brown, J. Chem. Phys. **86**, 1542 (1987).
[3] R. Edberg, G. P. Morriss, and D. J. Evans, J. Chem. Phys. **86**, 4555 (1987).
[4] G. P. Morriss, P. J. Daivis, and D. J. Evans, J. Chem. Phys. **94**, 7420 (1991).
[5] S. Chynoweth, U. C. Klomp, and Y. Michopoulos, J. Chem. Phys. **95**, 3024 (1991).
[6] P. Padilla and S. Toxvaerd, J. Chem. Phys. **97**, 7687 (1992).
[7] A. Berker, S. Chinoweth, U. C. Klomp, and Y. Michopoulos, J. Chem. Soc. Faraday Trans. **88**, 1719 (1992).
[8] P. J. Daivis and D. J. Evans, J. Chem. Phys. **100**, 541 (1994).
[9] M. E. Tuckerman, B. J. Berne, and G. J. Martyna, J. Chem. Phys. **97**, 1990 (1992).
[10] M. Watanabe and M. Karplus, J. Chem. Phys. **99**, 8063 (1993).
[11] C. J. Mundy, J. I. Siepmann, and M. L. Klein, J. Chem. Phys. **102**, 3376 (1995).
[12] Z. Xu, J. J. Depablo, and S. Kim, J. Chem. Phys. **102**, 5836 (1995).
[13] D. J. Evans and G. P. Morriss, *Statistical Mechanics of Nonequilibrium Liquids* (Academic, New York, 1990).
[14] P. T. Cummings and D. J. Evans, Ind. Eng. Chem. Res. **31**, 1237 (1992).
[15] K. P. Travis, P. J. Davis, and D. J. Evans, J. Chem. Phys. **103**, 1109 (1995).
[16] J. I. Siepmann, S. Karaborni, and B. Smit, Nature **365**, 330 (1993).
[17] B. Smit, S. Karaborni, and J. I. Siepmann, J. Chem. Phys. **102**, 2126 (1995).
[18] W. L. Jorgensen, J. D. Madura, and C. J. Swenson, J. Am. Chem. Soc. **106**, 6638 (1984).
[19] G. J. Martyna, M. L. Klein, and M. E. Tuckermann, J. Chem. Phys. **97**, 2635 (1992).
[20] D. Brown and J. H. R. Clarke, J. Chem. Phys. **92**, 3062 (1990).
[21] D. J. Evans, J. Stat. Phys. **20**, 547 (1979).
[22] D. J. Evans, Mol. Phys. **37**, 1745 (1979).
[23] S. T. Cui, P. T. Cummings, and H. D. Cochran, Mol. Phys. (submitted).
[24] K. Kawasaki and J. D. Gunton, Phys. Rev. A **8**, 2048 (1973).
[25] T. Yamada and K. Kawasaki, Prog. Theor. Phys. **53**, 111 (1975).
[26] M. H. Ernst, B. Cichocki, J. R. Dorfman, J. Sharma, and H. van Beijeren, J. Stat. Phys. **18**, 237 (1978).
[27] J. O. Rawlings, *Applied Regression Analysis* (Wadsworth and Brooks, Pacific Grove, 1988).
[28] P. T. Cummings and G. P. Morriss, J. Phys. F **18**, 1439 (1988).
[29] K. Stephan and K. Lucas, *Viscosity of Dense Fluids* (Plenum, New York, 1979).
[30] D. J. Evans, Phys. Lett. A **74**, 229 (1979).
[31] D. J. Evans, Phys. Rev. A **23**, 1988 (1981).
[32] D. J. Evans and H. J. M. Hanley, Physica A **108**, 567 (1981).
[33] D. J. Evans, Physica A **118**, 51 (1983).
[34] G. Ciccotti and J. P. Ryckaert, Comp. Phys. Rep. **4**, 345 (1986).
[35] G. Maréchal and J.-P. Ryckaert, Chem. Phys. Lett. **101**, 548 (1983).
[36] M. P. Allen, Mol. Phys. **52**, 705 (1984).